Optical, Field-Emission, and Antimicrobial Properties of ZnO Nanostructured Films Deposited at Room Temperature by Activated Reactive Evaporation

D. Yuvaraj,*,† R. Kaushik,‡ and K. Narasimha Rao†

Department of Instrumentation and Solid State and Structural Chemistry Unit, Indian Institute of Science, Bangalore, India

ABSTRACT ZnO nanostructures were deposited on flexible polymer sheet and cotton fabrics at room temperature by activated reactive evaporation. Room-temperature photoluminescence spectrum of ZnO nanostructured film exhibited a week intrinsic UV emission and a strong broad yellow-orange visible emission. TEM and HRTEM studies show that the grown nanostructures are crystalline in nature and their growth direction was indentified to be along [002]. ZnO nanostructures grown on the copper-coated flexible polymer sheets exhibited stable field-emission characteristics with a threshold voltage of 2.74 V/μm (250 μA) and a very large field enhancement factor (β) of 23,213. Cotton fabric coated with ZnO nanostructures show an excellent antimicrobial activity against *Staphylococcus aureus* bacteria (Gram positive), and ~73% reduction in the bacterial population is achieved compared to uncoated fabrics after 4 h in viability. Using a shadow mask technique, we also selectively deposited the nanostructures at room temperature on polymer substrates.

KEYWORDS: activated reactive evaporation • gas phase growth • ZnO nanostructures • field-emission studies • cotton fabrics and antibacterial property

1. INTRODUCTION

Zinc oxide (ZnO), a II−VI semiconductor has attracted greater attentions in the past few decades because of its interesting physical and chemical properties (1). Nanostructures of ZnO with different morphologies have been synthesized and investigated for possible application in solar cells, sensors, field-emission displays, light-emitting diodes, UV lasers, etc. (2, 3). In recent years, there have been numerous reports on the growth of a variety of ZnO nanostructures by physical vapor deposition (PVD), Chemical vapor deposition (CVD) and solution techniques (4–6). The requirement of high processing temperature, crystalline substrates, metal catalyst, seed layers, and longer growth times are the general drawbacks of the conventionally used growth techniques. The development of new products such as smart cloth and flexible displays requires the growth of nanostructures on cotton fabrics and polymer sheets (7, 8). As these substrates are highly unstable at high temperatures and harsh chemical environments, they require special techniques for the nanostructure growth. Currently growth of the ZnO nanostructure on cotton fabrics and polymer sheets are mainly carried out by different solution techniques. Vigneshwaran et al. have grown ZnO nanostructures on cotton fabrics by a novel pad-dry-cure method (9). Perelshtein et al. have synthesized ZnO nanostructures on cotton fabrics using ultra sound irradiation technique (10). El-Naggar et al. have deposited ZnO nanostructures on cotton and polyester fabrics by radiation and thermal treatment method (11).

Presently, ZnO nanostructures on polymer substrates for different applications such as flexible light-emitting diode and flexible field-emission devices have been synthesized mostly by solution roots (12, 13). (Table 1 in the Supporting Information show the different techniques which are presently employed for the growth of nanostructures on polymer substrates). The solution growth technique involves longer growth time and complicated multistep process. Earlier, we reported the deposition of ZnO nanostructured film at room temperature without using catalyst and template by activated reactive evaporation (ARE) (14, 15). In the ARE technique, nanostructures are grown in the gas phase and deposited as nanostructured film on the substrates placed above the plasma source.

The aim of this report is to explore the different possible applications of the ARE process in the area of nanotechnology. Using this process, we deposited ZnO nanostructures on rather uncommon substrates such as cotton fabrics and copper-coated polyethylene terephthalate sheets (Cu/PET). Using a shadow mask, we also selectively deposited ZnO nanostructures in a single step on PET sheets at room temperature. ZnO nanoneedles grown on Cu/PET sheet show stable field-emission characteristics with high field-enhancement factor (β), hence they have the potential to be used as cathode for flexible field-emission displays (FFED).

* Corresponding author.
Received for review November 14, 2009 and accepted March 1, 2010
† Department of Instrumentation, Indian Institute of Science.
‡ Solid State and Structural Chemistry Unit, Indian Institute of Science.
DOI: 10.1021/am900792k

Cotton fabrics coated with ZnO nanostructures by the ARE process show excellent antibacterial activity against *Staphylococcus aureus* (Gram positive) bacteria. The optical and structural properties of these grown nanostructured films were also characterized by XRD, SEM, TEM, and PL.

2. EXPERIMENTAL SECTION

In the present study, ZnO nanostructured films were deposited by ARE at room temperature on Cu/PET sheet, cotton fabrics, and on selected area of PET sheets by using a shadow mask (a schematic of the deposition chamber is shown in Figure I in the Supporting Information). Zinc metal beads (Aldrich 99.99%) were resistively evaporated at 48−55 Å/s from a perforated tantalum boat. An Ebert type hollow cathode (Al) discharge tube maintained at a potential of 800 V with a discharge current of 100 mA was used to ionize the oxygen gas during deposition (14). The partial pressure of oxygen during deposition was maintained at $2-3 \times 10^{-3}$ mbar by regulating the oxygen flow into the chamber by a needle valve. Evaporation of zinc at 48−55 Å/s through oxygen plasma generated by the discharge tube resulted in the growth of ZnO nanostructures in the gas phase, and they were then deposited as nanostructured films at room temperature on the substrates placed above the plasma source. TEM copper grid (200 mesh) and photochemical milled steel mask (thickness 100 μm) with the desired pattern were used as shadow mask for the selective deposition. These shadow masks were kept in close physical contact with the PET sheet by a clip arrangement, and nanostructures were then deposited at room temperature.

The structural properties of the nanostructured films were analyzed by X-ray diffraction (XRD, Phillips PW-1050/70 X-ray diffractometer with Cu Kα as the source) and the morphology and composition was examined by scanning electron microscopy attached with energy-dispersive X-ray analysis (EDAX) (SEM, ESEM Quanta). High-resolution transmission electron microscopy (HRTEM, Tecnai F-30) was employed to characterize the microstructural properties of the nanostructures. For the microstructural studies, nanostructured films on glass substrates were scraped by using a doctor blade, and this scraped powder was transferred to an ampule containing acetone. After ultrasonication for a few minutes, a few drops of this solution were carefully transferred into the holey-copper grids coated with carbon. This copper grid was stored and dried in vacuum using filament lamps and then transferred to the TEM chamber for microscopy studies. The PL Spectra of the ZnO nanostructured film and Cu/PET sheet was recorded at room temperature by ocean optics spectrophotometer using He−Cd (325 nm) as the excitation source. The field emission (FE) characteristic of the ZnO nanostructures deposited on Cu/PET sheet was measured in a two-parallel-plate configuration. Initially, the vacuum chamber was pumped to 2×10^{-5} mbar and then the chamber was purged with argon gas to remove any residual gases such as oxygen from the chamber. The voltage was swept manually between the electrodes using a keithley 2400 source meter from 0 to 500 V to test any short circuit between the electrodes. After this test, the voltage was swept using the automatic sweep option in the sourcemeter from 0 to 1100 voltages. This experiment was repeated a few times to check the consistence of the results. For antimicrobial studies, *Staphylococcus aureus* bacteria were cultured in a nutrient broth at 37 °C overnight in a mechanical shaker. The cultured microbial concentration was further reduced to 1×10^8 CFU/ml by serial dilution technique. The test samples were prepared by taking 9.9 mL of the sterile saline solution with 0.1 mL of inoculum. To study the antimicrobial activity of ZnO nanostructures, 1 cm^2 cotton fabrics coated with and without ZnO nanostructure were placed in the test tube containing microorganism at 37 °C for 4 h in a shaker. Then, 100 μL of the test solution was taken and plated in a nutrient agar plate and incubated at 37 °C. Bacterial colonies were counted after 24 h and the antibacterial activity due to ZnO nanostructures was determined.

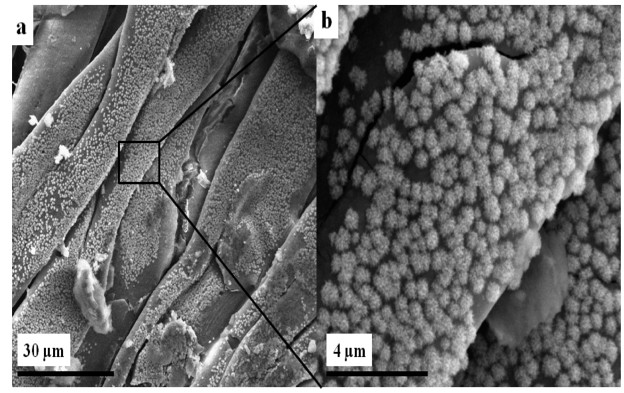

FIGURE 1. (a, b) Low- and high-magnification SEM image of the ZnO nanostructures deposited on cotton fabrics.

3. RESULTS AND DISCUSSION

3.1. Deposition of ZnO Nanostructure on Cotton Fabrics and PET Sheets. Figure 1 a, b shows the low- and high-magnification SEM image of the ZnO nanostructures grown on the cotton fabrics. The morphology consists of large number of needlelike nanostructures oriented in a random manner. Similarly, ZnO nanostructures were also grown on the Cu/PET. (Figure II in the Supporting Information shows the SEM images of the dense ZnO nanostructures grown on polymer substrates). These SEM images indicates the versatility of the ARE technique to deposit nanostructures over a range of substrates such as polymer, Cu/PET, and cotton fabrics. Chemical composition of the nanostructures measured using EDAX has shown the presence of the zinc and oxygen only.

3.2. Structural Studies. XRD studies show that the nanostructures grown on cotton fabrics and polymer substrates crystallize in ZnO wurtzite structures. This XRD pattern have shown peaks corresponding to peak (100), (002), and (101) of ZnO. (XRD pattern of the ZnO nanostructured film is shown in Figure III in the Supporting Information). No other peak corresponding to source material, other impurities and phases were observed in the XRD pattern. The microstructural property of the ZnO nanoneedle was characterized by TEM. Figure 2a shows the low-magnification TEM image of the nanoneedles dispersed on the TEM copper grid. The low-magnification TEM image shows that the nanoneedles have smooth edges and are free from catalytic particles. The HRTEM image of the marked region in Figure 2a is shown in Figure 2b. The clear lattice fringes in the HRTEM image show the crystallinity of the ZnO nanoneedles. The lattice fringes observed along the growth direction of the ZnO nanoneedles with a spacing of 0.26 nm correspond to the *d*-spacing of the (002) of wurtzite ZnO. This observation shows ZnO nanoneedle preferential grow along the [002] direction. The chemical composition of the ZnO nanoneedle was measured by EDAX during TEM analysis from the tip to the base. The EDAX spectrum of the

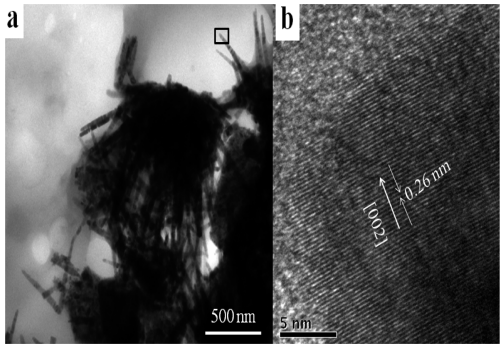

FIGURE 2. (a) Low-magnification TEM image of the ZnO nanoneedles, (b) HRTEM image of the ZnO nanoneedle tip, with a spacing of 0.26 nm between the adjacent lattice fringes.

nanoneedle indicates the presence of Zn and O only with an atomic ratio of ~1.

3.3. PL Studies. Figure 3a shows the photoluminescence spectrum of ZnO nanostructured film and Cu/PET substrate recorded at room temperature. The PL spectrum of the Cu/PET sheet does not show any significant peak and hence all the peaks in Figure 3a are attributed to that of the ZnO film. The PL spectrum of the ZnO nanostructured film consists of two peaks centered at 389.7 and 590 nm. The weak narrow peak at 389.7 nm in the U.V region is attributed to the near band edge emission, whereas the broad peak from 475 to 700 nm centered at 590 nm (yellow-orange region) is attributed to defect emission. Although there are several reports on the PL emission of ZnO nanostructures, the origin of the visible emission is still not clear. Djurisic et al. have reported that the yellow emission in the solution-grown ZnO nanostructures occurs due to the hydroxyl group present on the surface of the nanostructures (16). Formation of defects in the nanoparticles during milling also resulted in the broad yellow-orange emission and the intensity of the visible emission was found to decrease with time because of aging (17). In addition to this, the presence of oxygen interstitial and impurities such as Li and Mn ions in ZnO are attributed as the possible reason behind the occurrence of yellow emission (18).

FTIR studies on the ZnO nanostructure coated on Cu/PET sheets indicated the absences of hydroxyl group on the surface. Hence within the detection limits of FTIR and EDAX we have not observed any higher level of impurities in the grown nanostructures, so observed broad yellow-orange emission may be due to the presence of some intrinsic defects. Further investigation will be continued to find the origin of the visible emission and will be reported elsewhere. The higher intensity of the visible emission compared to the U.V emission (Figure 3a) shows that these nanostructures have higher defect concentration. The higher level of defect associated with the nanostructures in this film is attributed to the low deposition temperature and the fast and gas-phase growth process. The PL spectrum of the ZnO nanostructured films was also measured at different laser excitation powers. Figure 3b shows the intensity ratio of the visible to UV PL emission peaks at different laser excitation power. This ratio increase with the decrease in the laser power, i.e., the intensity of the visible emission peak becomes dominant with the decrease in the laser excitation power, contradictory to the result reported by Djurisic et al., where the intensity of the visible emission peak is saturated with the decrease in the excitation power (19). This visible dominant PL emission even at low excitation power occurs because of the high density of the defects present in the gas-phase-grown nanostructures. Furthermore, no shift in the peak position of the UV and visible emission is observed with the variation in the excitation laser power.

3.4. Field-Emission Studies. Recently one-dimensional (1D) ZnO nanostructures of different morphologies such as nanotubes, nanowires, nanobelts, and nanoneedles have been synthesized and tested for FE application. Among the various morphologies, nanoneedles exhibit good FE properties because of their sharp apexes, large aspect ratios, and good alignment on the substrate (20). Although there are several reports on field-emission studies of ZnO nanostructures, relatively few studies have been carried out on the field-emission properties of ZnO nanostructures grown on flexible substrates (21–23).

Figure 4a shows the FE curves of the current density versus the applied field ($J-E$) for the ZnO nanoneedles grown on Cu/PET, with a cathode−anode spacing of 180 μm. The synthesized samples had a turn on field of 1.17 V/μm (10 μA) and threshold field of 2.74 V/μm (250 μA). Figure 4b shows the Fowler−Nordheim (F−N) plot of the $J-E$ curves, i.e., $\ln(J/E^2)$ vs $1/E$, for the ZnO nanostructures grown on Cu/PET substrate. From this figure, it is observed that the F−N plot exhibits a two slope behavior. This type of nonlinearity in the F−N plot has been reported for other systems also (24, 25). However, the mechanism of the multistage slope phenomena is not clear yet, and it has been explained on the basis of the energy band, adsorbents, and defects (26). F−N plots having two slopes in the present study resembles the work reported by Ramgir et al. (i.e., smaller and larger value of slope in the low and high field regions, respectively) (27). They have explained the two slope behavior based on the electron emission from Conduction (CB) and valence band (VB). In the low-field range, the electron emission occurs from the CB only. However, when the applied field is increased further, additional emission from the VB, i.e., 3.3 eV below the CB also starts contributing to the emission current along with the emission from the CB. And the β value calculated using the increased work function of 8.67 eV ($\varphi_0 = \varphi + E_g$) by Ramgir et al. agreed well with the β value calculated in the low-field region values. But in the present study, different values were observed. Hence based on the larger number of data points present in the high-field region, the slope is measured in the high-field region by plotting a straight line as shown in Figure 4b.

According to the F−N theory, the slope of the F−N plots is equal to $-6830\,\varphi^{3/2}/\beta$, where φ is the work function and β the enhancement factor. Taking $\varphi = 5.3$ eV for ZnO (28), we calculated the β value and found it to be ~23 213 for the ZnO nanoneedles grown on the Cu/PET substrate. The β value obtained in this study is greater than the reported value for CNT grown on flexible Co/Cr/TEFLON sheet by

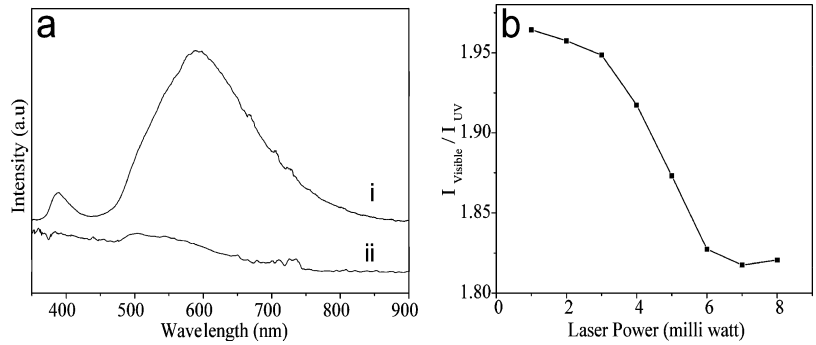

FIGURE 3. (a) (i, ii) PL spectra of the ZnO nanostructured films coated and bare Cu/PET sheet. (b) Variation in the intensity ratio of the visible to UV light with the incident laser power.

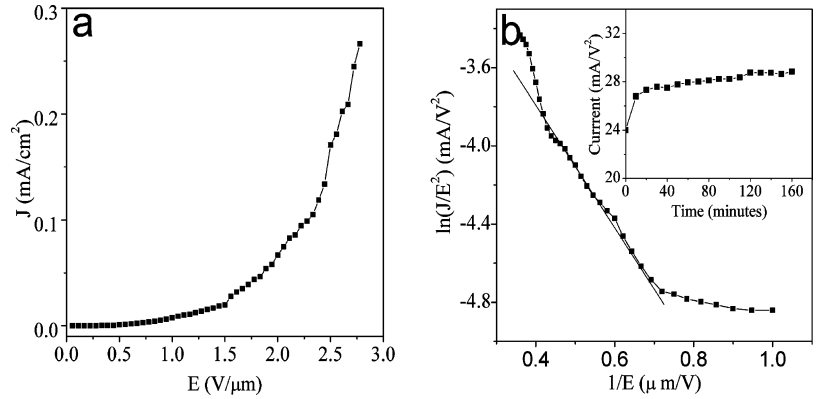

FIGURE 4. (a) Field-emission current density-applied field ($J-E$) plot of the ZnO nanostructure grown on Cu/PET. (b) Fowler–Nordheim (F–N) plot of the ZnO nanostructures grown on Cu/PET. (Inset) Field-emission current measured as a function of time under a constant applied field of 10 V/μm.

Yoon et al. (22), ZnO nanowires grown on polystyrene sheets by Cui et al. (23), and nanoneedles grown by Yang et al. on Polyimide foil (21). The field-emission property of nanostructure depends on the geometry of the nanostructures, the electrical contact between the nanostructures, aerial density of the nanostructures, and cleanliness of the surface (20). In the present work, the nanoneedles have a sharper tip than the faceted nanowires (the high aspect ratio as calculated from the TEM image in Figure 2 was found to be ~35). The calculated value of β in the present work is higher than the values reported for sharp nanoneedles grown on bare Si substrates by vapor phase growth (29). This may be due to the improvised electrical contacts between the ZnO nanostructures and Cu film than between ZnO nanostructures and bare Si substrate. The field enhancement factor (β) of the nanoneedles grown by ARE in the present work is greater than the similar type of nanostructures grown on different substrates such as Si, ITO/glass and Cu/Si by solution technique (30, 31). This is mainly because the surface of the nanostructures grown in the vacuum are free from organic surfactants and hydroxyl groups and hence have better field-emission characteristics than the nanostructures grown by solution and low vacuum catalyst assisted (VLS) process (32). The stability of the emission from the nanostructures was tested and the inset in Figure 4b shows the field-emission current measured as a function of time under the constant voltage of (300 V) and distance of 180 μm between the electrodes. The field-emission current does not fluctuate much, and moreover, the current slightly increased with time, from 24 μA at the starting point to 28.85 μA at the end of the 160th minute. The increase in the emission current with time might be due to desorption of the absorbed oxygen molecules from the surface during the continuous emission process (33).

3.5. Antibacterial Activity. Different inorganic nanostructures are effective against the growth of bacteria. These nanostructures have several advantages than the organic fungicides. They are nontoxic and can withstand high temperature and harsh environments. Metal nanoparticles such as Ag and Au are well-known for their antimicrobial activity. In addition to these metal nanoparticles, metal oxide nanostructures such as ZnO, TiO_2, and CuO have been reported as effective antimicrobial agents (9, 10). In the present, work antibacterial activity of the plain cotton fabrics and cotton fabrics coated (deposited) with ZnO nanostructures was tested using *Staphylococcus aureus* bacterium (Gram positive). Fabrics coated with nanostructures reduced the number of bacterial colonies by ~73% when compared to the plain fabrics after 4 h treatment in viability. Perelshtein et al. have reported that the antibacterial activity of ZnO nanostructures is due to the formation of the oxygen radicals, which effectively prevents the growth of *Staphylococcus aureus* bacterium on cotton cloth. Zone of inhibition was carried out with Muller Hinton agar medium (Kirby–Bauer method) by placing a small piece of nanofabric over a bacterial lawn. These ZnO nanostructures effectively prevented the growth of bacteria on the cloth and resulted in

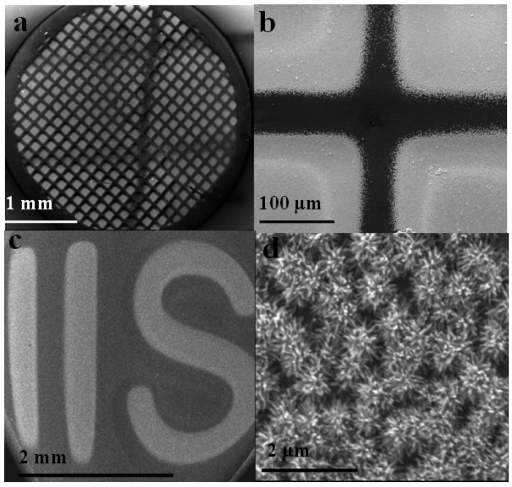

FIGURE 5. (a−c) Micropatterns selectively deposited on polymer substrates using TEM copper grid and photochemically milled mask. (d) High-magnification SEM image of the ZnO nanostructured film deposited on polymer substrates.

the formation of a zone around the nanofabrics (photographic images of the antibacterial activity and zone of inhibition due to ZnO/fabrics are shown in Figure IV in the Supporting Information).

3.6. Selective Deposition of ZnO Nanostructures. Application of nanomaterials for the fabrication of different devices such gas sensors, UV lasers, solar cells, and field-emission display requires the growth of aligned nanostructures in the form of patterns. Hence much of the current activities in nanostructure synthesis are focused on achieving aligned and patterned growth of nanostructures. Selective growth of ZnO nanostructures on different substrates such as Si, quartz, sapphire, and GaN with nanometer resolution have been realized by different techniques such as photolithography, electron beam lithography, scanning probe lithography, nanosphere lithography, and self-assembly (34–36). As polymer substrates have low melting points and are chemically reactive, the above-mentioned techniques are not applicable for the selective growth of ZnO nanostructures on polymer substrates. Selective growth of nanostructures on polymer substrates has been realized by selective functionalization of the polymer surfaces and pattern transfer methods (37, 38). Even though there are many developments in the area of patterned nanostructure growth, in general all these techniques involve tedious multistep processes. Application of the patterned nanostructures for the fabrication of practical nanoscale devices can only be realized if the growth can be carried out in a simple and cost-effective manner over a larger area.

ZnO nanostructured films containing needlelike structures were deposited on the selected area by using a shadow mask on flexible polymer substrates. A low-magnification SEM image of the ZnO nanostructured film deposited on polymer substrate using a TEM copper grid and a photochemical milled mask having the letter 'IIS' is shown in Figure 5a−c, respectively. The micropatterns deposited using these mask had well-defined edges, and each micropattern contain needlelike nanostructures. The smallest micropattern attained using this technique measured about 90 μm. Variety of micro patterns with smaller feature sizes can be realized in the future by using a shadow mask fabricated by other sophisticated techniques (39).

4. CONCLUSION

ZnO nanostructures were successfully deposited in a single step at room temperature on variety of substrates such as Cu/PET, cotton fabrics and on selected area of PET sheets by ARE technique. The photoluminescence spectra of these films show a week UV emission and a broad yellow orange emission. TEM studies indicate that the gas phase grown ZnO nanoneedles are crystalline in nature and their growth direction was found to be along [002]. ZnO nanostructures deposited on flexible Cu/PET substrates have shown a low turn on (10 μA), a threshold field (250 μA) of 1.17 and of 2.74 V/μm, respectively, and a very high field-enhancement factor (β) of 23 133. The field-emission characteristics of these films promise to be a good candidate for low-cost, flexible field-emission display (FFED) application. Cotton fabrics deposited with ZnO nanostructures show a reduction of ∼73% against *Staphylococcus aureus* bacterial population when compared to a plain cotton fabric after 4 h in viability.

Acknowledgment. The authors thank Dr. Venugopal Achanta, Tata Institute of Fundamental Research (TIFR), Mumbai, and Prof. S. Ashokan, Department of Instrumentation, Indian Institute of Science, Bangalore, for their help in carrying out experiments on the PL and FE studies.

Supporting Information Available: Additional information and figures (PDF). This material is available free of charge via the Internet at http://pubs.acs.org.

REFERENCES AND NOTES

(1) Ozgur, U.; Alivov, Y. I.; Liu, C.; Teke, A.; Reshchikov, M. A.; Dogan, S.; Avrutin, V.; Cho, S. J.; Morkoc, H. *J. Appl. Phys.* **2005**, *98*, 041301.
(2) Wang, Z. L. *J. Phys.: Condens. Matter* **2004**, *16*, R829.
(3) Schmidt-Mende, L.; MacManus-Driscoll, J. L. *Mater. Today* **2007**, *10*, 40.
(4) Yao, B. D.; Chan, Y. F.; Wang, N. *Appl. Phys. Lett.* **2002**, *81*, 757.
(5) Umar, A.; Lee, S.; Im, Y. H.; Hahn, Y. B. *Nanotechnology* **2005**, *16*, 2462.
(6) Gonzalez-Valls, I.; Lira-Cantu, M. *Energy Environ. Sci.* **2009**, *2*, 19.
(7) Durán, N.; Marcato, P. D.; De Souza, G. I. H.; Alves, O. L.; Esposito, E. *J. Biomed. Nanotechnol.* **2007**, *3*, 203.
(8) Lee, O. J.; Lee, K. H. *Appl. Phys. Lett.* **2003**, *82*, 3770.
(9) Vigneshwaran, N.; Kumar, S.; Kathe, A. A.; Varadarajan, P. V.; Prasad, V. *Nanotechnology* **2006**, *17*, 5087.
(10) Perelshtein, I.; Applerot, G.; Perkas, N.; Wehrschetz-Sig, E.; Hasmann, A.; Guebitz, G. M.; Gedanken, A. *Appl. Mater. Interface* **2009**, *1*, 361.
(11) El-Naggar, A. M.; Zohdy, M. H.; Hassan, M. S.; Khalil, E. M. *J. Appl. Polym. Sci.* **2003**, *88*, 1129.
(12) Liu, T. Y.; Liao, H. C.; Lin, C. C.; Hu, S. H.; Chen, S. Y. *Langmuir* **2006**, *22*, 5804.
(13) Pradhan, D.; Kumar, M.; Ando, Y.; Leung, K. T. *J. Phys. Chem. C* **2008**, *112*, 7093.
(14) Yuvaraj, D.; Rao, K. N.; Nanda, K. K. *J. Phys. D: Appl. Phys.* **2009**, *42*, 035403.
(15) Yuvaraj, D.; Nanda, K. K.; Rao, K. N. *Curr. Nanosci.* **2009**, *5*, 283.
(16) Djurisic, A. B.; Leung, Y. H.; Tam, K. H.; Ding, L.; Ge, W. K.; Chen, H. Y.; Gwo, S. *Appl. Phys. Lett.* **2006**, *88*, 103107.
(17) Radoi, R.; Fernandez, P.; Piqueras, J.; Wiggins, M. S.; Solis, J. *Nanotechnology* **2003**, *14*, 794.
(18) Djurisic, A. B.; Leung, Y. H. *Small* **2006**, *2*, 944.

(19) Djurisic, A. B.; Choy, W. C. H.; Roy, V. A. L.; Leung, Y. H.; Kwong, C. Y.; Cheah, K. W.; Rao, T. K. G.; Chan, W. K.; Lui, H. F.; Surya, C. *Adv. Funct. Mater.* **2004**, *14*, 856.
(20) She, J.; Xiao, Z.; Yang, Y.; Deng, S.; Chen, J.; Yang, G.; Xu, N. *ACS Nano* **2008**, *2*, 2015.
(21) Yang, H. Y.; Lau, S. P.; Yu, S. F.; Huang, L.; Tanemura, M.; Tanaka, J.; Okita, T.; Hng, H. H. *Nanotechnology* **2005**, *16*, 1300.
(22) Yoon, B. J.; Hong, E. H.; Jee, S. E.; Yoon, D. M.; Shim, D. S.; Son, G. Y.; Lee, Y. J.; Lee, K. H.; Kim, H. S.; Park, C. G. *J. Am. Chem. Soc.* **2005**, *127*, 8234.
(23) Cui, J. B.; Daghlian, C. P.; Gibson, U. J.; Püsche, R.; Geithner, P.; Ley, L. *J. Appl. Phys.* **2005**, *97*, 044315.
(24) Zhang, X.; Zhang, G.; Bai, X.; Zhao, X.; Xiao, J.; Wu, Y.; Lu, F.; Guo, D. *J. Vac. Sci. Technol., B* **2009**, *27*, 705.
(25) Liu, N.; Fang, G.; Zeng, W.; Long, H.; Yuan, L.; Zhao, X. *Appl. Phys. Lett.* **2009**, *95*, 153505.
(26) Xu, C. X.; Sun, X. W.; Fang, S. N.; Yang, X. H.; Yu, M. B.; Zhu, G. P.; Cui, Y. P. *Appl. Phys. Lett.* **2006**, *88*, 161921.
(27) Ramgir, N. S.; Late, D. J.; Bhise, A. B.; Mulla, I. S.; More, M. A.; Joag, D. S.; Pillai, V. K. *Nanotechnology* **2006**, *17*, 2730.
(28) Pradhan, D.; Kumar, M.; Ando, Y.; Leung, K. T. *Appl. Mater. Interface* **2009**, *1*, 789.
(29) Marathe, S. K.; Koinkar, P. M.; Ashtaputre, S. S.; More, M. A.; Gosavi, S. W.; Joag, D. S.; Kulkarni, S. K. *Nanotechnology* **2006**, *17*, 1932.
(30) Cao, B.; Teng, X.; Heo, S. H.; Li, Y.; Cho, S. O.; Li, G.; Cai, W. *J. Phys. Chem. C* **2007**, *111*, 2470.
(31) Xu, C. X.; Sun, X. W.; Fang, S. N.; Yang, X. H.; Yu, M. B.; Zhu, G. P.; Cui, Y. P. *Appl. Phys. Lett.* **2006**, *88*, 161921.
(32) Chen, H.; Qi, J.; Zhang, Y.; Zhang, X.; Liao, Q.; Huang, Y. *Appl. Surf. Sci.* **2007**, *253*, 8901.
(33) Yeong, K. S.; Maung, K. H.; Thong, J. T. L. *Nanotechnology* **2007**, *18*, 185608.
(34) Chung, T. F.; Luo, L. B.; He, Z. B.; Leung, Y. H.; Shafiq, I.; Yao, Z. Q.; Lee, S. T. *Appl. Phys. Lett.* **2007**, *91*, 233112.
(35) Fan, H. J.; Fuhrmann, B.; Scholz, R.; Syrowatka, F.; Dadgarc, A.; Krostc, A.; Zachariasa, M. *J. Cryst. Growth* **2006**, *287*, 34.
(36) Ito, D.; Jespersen, M. L.; Hutchison, J. E. *ACS Nano* **2008**, *2*, 2001.
(37) Morin, S. A.; Amos, F. F.; Jin, S. *J. Am. Chem. Soc.* **2007**, *129*, 13776.
(38) Weintraub, B.; Deng, Y.; Wang, Z. L. *J. Phys. Chem. C,* **2007**, *111*, 10162.
(39) Kim, G. M; Van den Boogaart, M. A. F.; Brugger, J. *Microelectron. Eng.* **2003**, *67*, 609.

AM900792K